Published in final edited form as:
J Comp Neurol. 2011 April 1; 519(5): 989–1005. doi:10.1002/cne.22563.

Differential Structural Plasticity of Corticostriatal and Thalamostriatal Axo-Spinous Synapses in MPTP-Treated Parkinsonian Monkeys

Rosa M. Villalba[1,*] and **Yoland Smith**[1,2]

[1]Yerkes National Primate Research Center, Emory University, Atlanta, Georgia 30329

[2]Department of Neurology; Emory University, Atlanta, Georgia 30329

Abstract

Striatal spine loss is a key pathological feature of Parkinson's disease (PD). Knowing that striatal glutamatergic afferents target dendritic spines, these data appear difficult to reconcile with evidence for an increased expression of the vesicular glutamate transporter 1 (vGluT1) in the striatum of PD patients and 1-methyl-4-phenyl-1,2,3,6-tetrahydropyridine (MPTP)-treated monkeys, as well as in some electrophysiological studies showing overactivity of the corticostriatal glutamatergic system in models of parkinsonism. To address the possibility that structural changes in glutamatergic afferents may underlie these discrepancies, we undertook an ultrastructural analysis of vGluT1-positive (i.e., corticostriatal) and vGluT2-positive (i.e., mostly thalamostriatal) axo-spinous glutamatergic synapses using a 3D electron microscopic approach in normal and MPTP-treated monkeys. Three main conclusions can be drawn: 1) spines contacted by vGluT1-containing terminals have larger volume and harbor significantly larger postsynaptic densities (PSDs) than those contacted by vGluT2-immunoreactive boutons; 2) a subset of vGluT2-, but not vGluT1-immunoreactive, terminals display a pattern of multisynaptic connectivity in normal and MPTP-treated monkeys; and 3) VGluT1- and vGluT2-positive axo-spinous synapses undergo ultrastructural changes (larger spine volume, larger PSDs, increased PSD perforations, larger presynaptic terminal) indicative of increased synaptic activity in parkinsonian animals. Furthermore, spines contacted by cortical terminals display an increased volume of their spine apparatus in MPTP-treated monkeys, suggesting an increased protein synthesis at corticostriatal synapses. These findings demonstrate that corticostriatal and thalamostriatal glutamatergic axo-spinous synapses display significantly different ultrastructural features, and that both systems undergo complex morphological changes that could underlie the pathophysiology of corticostriatal and thalamostriatal systems in PD.

Keywords

dopamine; glutamate; vesicular glutamate transporters; electron microscopy; dendritic spine; 3D-reconstruction

One of the main neuropathological features of Parkinson's disease (PD) is the degeneration of the nigrostriatal dopaminergic pathway, which induces complex physiological changes

[*]CORRESPONDENCE TO: Rosa M. Villalba, Ph.D., Yerkes National Primate Research Center, Emory University, 954 Gatewood Rd. NE, Atlanta, GA 30329. rvillal@emory.edu.

Additional Supporting Information may be found in the online version of this article.

within the basal ganglia circuitry, including profound alterations in the activity of the corticostriatal glutamatergic system (Calabresi et al., 1996, 2007; Mallet et al., 2006; Wichmann and DeLong, 2007). The anatomical substrate and mechanism by which dopamine (DA) regulates striatal glutamatergic activity is complex and activity dependent and remains poorly understood (Smith and Bolam, 1990; Bamford et al., 2004; Calabresi et al., 2007; Surmeier et al., 2007; Ballion et al., 2008; Smith and Villalba, 2008; Tian et al., 2010). The most common targets where dopaminergic and glutamatergic striatal afferent systems functionally interact are the dendritic spines of striatofugal medium spiny neurons (MSNs) (Smith and Bolam, 1990). Most, if not all, cortical innervation of MSNs terminates on dendritic spines (Kemp and Powell, 1970; Raju et al., 2006).

Although not as extensive as the corticostriatal system, a significant contingent of thalamic glutamatergic afferents also targets dendritic spines and displays close relationships with dopaminergic terminals in the striatum (Raju et al., 2006; Moss and Bolam, 2008; Smith et al., 2009a,b). In both animal models of parkinsonism and PD patients, MSNs lose as much as 30–50% of the dendritic spines, which, in rats, is accompanied by a similar decrease in the total number of asymmetric glutamatergic synapses (Ingham et al., 1989, 1998; Stephens et al., 2005; Zaja-Milatovic et al., 2005; Day et al., 2006; Deutch et al., 2007; Neely et al., 2007; Scholz et al., 2008; Schuster et al., 2009; Smith et al., 2009b; Villalba et al., 2009; Garcia et al., 2010; Soderstrom et al., 2010). Despite this significant spine loss, some in vivo and in vitro electrophysiological studies have suggested increased activity of the corticostriatal system in parkinsonism (Galarraga et al., 1987; Calabresi et al., 1996; Marti et al., 1999), although this issue appears to be more complex than originally thought (Day et al., 2006; Mallet et al. 2006).

The vesicular glutamate transporters (vGluT) 1 and 2 provide unique tools to differentiate cortical from thalamic axon terminals in the striatum. In situ hybridization for vGluT1 and vGluT2 mRNA showed that vGluT1 signal predominates in the cerebral cortex (Fremeau et al., 2001, 2004; Herzog et al., 2001), whereas vGluT2 mRNA is most abundant in the thalamus (Fremeau et al., 2001, 2004; Herzog et al., 2001; Bacci et al., 2004; Hur and Zaborszky, 2005). Immunocytochemical studies from our laboratory and others have clearly shown that vGluT1 is confined to cortical boutons, whereas vGluT2 is a preferential, although not exclusive, marker of thalamic afferents in the rat and monkey striatum (Lacey et al., 2005; Raju and Smith, 2005; Raju et al., 2006, 2008).

Immunochemical studies have demonstrated an increased expression of vGluT1 in the striatum of 1-methyl-4-phenyl-1,2,3,6-tetrahydropyridine (MPTP)-treated parkinsonian monkeys (Raju et al., 2008) and postmortem striatal tissue of PD patients (Kashani et al., 2007). In addition, the striatum of DA-depleted rats contains a larger density of perforated asymmetric synapses (Ingham et al, 1998; Meshul et al., 1999, 2000), a form of structural remodeling associated with increased synaptic efficacy in other brain regions (Greenough et al., 1978; Bertoni-Freddari et al., 1993; Harris and Kater, 1994). Therefore, the overactivity of the corticostriatal glutamatergic system described by some authors in rodent models of parkinsonism might result from complex structural and neurochemical changes of glutamatergic axo-spinous synapses in dopamine-depleted striata.

To address this issue further, we used a three-dimensional (3D) electron microscopy reconstruction method to perform a rigorous quantitative analysis of the ultra-structural features of spines specifically targeted by thalamic or cortical afferents in the sensorimotor striatum of normal and MPTP-treated parkinsonian monkeys. Our data show that thalamostriatal and corticostriatal afferents target different types of striatal spines, and that both systems undergo complex, and partly different, ultrastructural changes indicative of an increased strength of glutamatergic transmission in parkinsonism.

MATERIALS AND METHODS

Animals and tissue preparation

A total of five control and five MPTP-treated adult rhesus monkeys (*Macaca mulatta*; Yerkes National Primate Research Center colony) were used in these studies. Brain tissue from these animals has been used in previous studies (Raju et al., 2008; Villalba et al., 2009). The housing, feeding, and experimental conditions used in these studies followed the guidelines of the National Institutes of Health's *Guide for the Care and Use of Laboratory Animals* and were approved by the institutional animal care and use committee of Emory University.

MPTP injections and parkinsonism

Before the MPTP treatment was started, the monkeys were first habituated to a behavioral observation cage, and a baseline of motor behavior was established. During the MPTP treatment, behavioral changes and parkinsonian motor signs were measured once a week over a 20-minute time period during a minimum of 6 months with quantitative methods that are routinely used in our laboratory (Soares et al., 2004; Bogenpohl et al., 2007; Kliem et al., 2009; Galvan et al., 2010). In two monkeys, MPTP (Sigma-Aldrich, St. Louis, MO) was injected unilaterally through the right carotid artery (total dose 2–3 mg/kg) under general isoflurane anesthesia (1–3%), whereas the other three animals received intramuscular injections of MPTP once a week until they displayed stable parkinsonian symptoms (total dose 4.3–8 mg/kg; Sigma-Aldrich). The parkinsonian motor signs were documented through observations of spontaneous cage behavior. A computer-assisted behavioral scoring system was used to quantify motor behaviors in the two animals that received intracarotid administration of MPTP.

Briefly, a computer keyboard key was assigned to a specific limb on the ipsilateral or contralateral side of the MPTP injection, and, each time the animal moved that limb, the key was pressed. Limb movements were documented over a 20-minute time period at least once every 2 weeks during a minimum of 6 months following the MPTP injection. Both monkeys displayed significant signs of parkinsonism in the arm and leg contralateral to the side of the intracarotid MPTP administration. In both animals the ratio of limb movements on the affected/nonaffected side ranged from 0.8 to 0.95 in the normal state and 0.1 to 0.28 in the stable parkinsonian condition. The limb movements on the side of the body ipsilateral to the intracarotid MPTP injections were not significantly affected.

In animals that received systemic MPTP injections, an automated activity monitoring system was used to quantify general motor activity. The observation cage was equipped with eight infrared beams (Banner Engineering, Minneapolis, MN) arranged in a square formation on two adjacent sides of the cage (back and side). The animal's behavior was also videotaped. A computer system was attached and logged the timing of beam crossings. Off-line, the total activity counts within a 20-minute period were calculated. Finally, a rating scale was used to determine the degree of behavioral change induced by MPTP treatment. Nine criteria were used to assess parkinsonian motor signs (gross motor activity, balance, posture, arm bradykinesia, arm hypokinesia, leg bradykinesia, leg hypokinesia, arm tremor, and leg tremor), each on a scale of 0 to 3 (normal/absent to severe), yielding a maximum score of 27. A score of 10 or more was considered as moderate parkinsonism.

The three animals that received systemic MPTP administration displayed moderate parkinsonian motor signs (total activity counts decreased by 60–73%; Unified Parkinson's Disease Rating Scale [UPDRS] counts range from 12 to 16) that remained stable for a period of at least 6 months before sacrifice. A monkey was considered stable parkinsonian if the score in the parkinsonian rating scale was at least 10, and if the counts in the activity

monitoring remained 60% or below the baseline levels for at least 6 weeks after the last MPTP injection (Galvan et al., 2010).

Animal perfusion

Animals were deeply anesthetized with an overdose of pentobarbital (100 mg/kg, iv) and perfused transcardially with cold oxygenated Ringer's solution, followed by 2 liters of fixative containing 4% paraformaldehyde and 0.1% glutaraldehyde in phosphate buffer (PB; 0.1 M, pH 7.4). After perfusion, the brains were removed from the skull and cut into 10-mm-thick blocks in the frontal plane. Tissue sections (60 μm thick) were obtained with a Vibratome, collected in cold phosphate-buffered saline (PBS; 0.01 M, pH 7.4), and treated with sodium borohydride (1% in PBS, 20 minutes). In the two unilaterally MPTP-treated monkeys, only the striatum on the ipsilateral side of the MPTP intracarotid injections was used for further analysis.

vGluT1 and vGluT2 immunostaining

Primary antibodies—Two polyclonal antibodies were used (Table 1), as follows:

1. Rabbit anti-rat vGluT1 antibody (Mab Technologies, Atlanta, GA). To generate this antibody, a peptide corresponding to amino acids 543–560 (CATHSTVQPPRPPPPVRDY) of the COOH terminus of the rat vGluT1 was used as antigen. The Western blot analysis with the anti-vGluT1 antibody showed a single band in monkey striatal tissue at ~60 kDa, corresponding to the molecular weight predicted for vGluT1, whereas the peptide preadsorption completely abolished striatal immunostaining (Villalba et al., 2006).
2. Rabbit anti-human vGluT2 antibody (Mab Technologies). The antiserum was obtained from rabbits (Covance, Princeton, NJ) immunized against a peptide corresponding to amino acids 560–578 (KKEEFVQGEVQDSHSYKDR) of the COOH terminus of the human vGluT2 (hvGluT2). The underlined amino acids are human specific. Following purification procedures, the specificity of vGluT2 antibody on monkey tissue was determined by Western immunoblots and light microscopy preadsorption immunohistochemical analyses as previously described by Raju et al. (2008). Western blot analysis identified a single band at ~65 kDa, as predicted for the vGluT2 protein in monkey. Further analysis at the light microscopic level showed that the neuropil was immunolabeled and preadsorption of the antibody by control peptide abolished immunolabeling, whereas preincubation of the anti-vGluT2 antibody with vGluT1 peptide had no effect on immunostaining (Raju et al., 2008).

Immunoperoxidase labeling for electron microscopy—Tissue sections from the postcommissural putamen in five control monkeys (animals C1–C5) and five animals (animals M1–M5) rendered parkinsonian following intracarotid (n = 2) or systemic (n = 3) MPTP injections were used in these studies. Table 2 describes the distribution of these 10 animals across the vGluT1 or vGluT2 immunostaining procedure in normal and MPTP-treated monkeys (Table 2). In brief, the striatal tissue of two different control and two different MPTP-treated monkeys was immunostained with the vGluT1 (animals C1, C3, M1, and M2) or vGluT2 (animals C4, C5, M4, and M5) antibodies, whereas the striatum of one control (animal C2) and one MPTP-treated (animal M3) monkey was used for both vGluT1 and vGluT2 immunostaining. Sections were placed in a cryoprotectant solution (PB; 0.05 M, pH 7.4, containing 25% sucrose and 10% glycerol) for 20 minutes, frozen at −80°C for 20 minutes, thawed, and returned to a graded series of cryoprotectant (100%, 70%, 50%, 30%) diluted in PBS. They were then washed in PBS before being processed for immunocytochemistry.

The sections were preincubated in a solution containing 10% normal goat serum and 1% bovine serum albumin in PBS for 1 hour. They were then incubated for 48 hours at 4°C with the antisera diluted at 0.2 μg/ml in a solution containing 1.0% normal goat serum (NGS) and 1.0% bovine serum albumin (BSA) in PBS. Next, the sections were rinsed in PBS and transferred for 1.5 hours to a secondary antibody solution containing biotinylated goat anti-rabbit IgGs (Vector, Burlingame, CA), diluted 1:200. After rinsing, sections were put in a solution containing 1% avidin-biotin-peroxidase complex (Vector). The tissue was then washed in PBS and Tris buffer (0.05 M pH 7.6) before being transferred into a solution containing 0.01 M-imidazole, 0.005% hydrogen peroxide, and 0.025% 3,3′-diaminobenzidine tetrahydrochloride (DAB; Sigma, St. Louis, MO) in Tris for 10 minutes. The DAB reaction was terminated with several rinses in PBS.

Following the immunostaining reactions, the sections were transferred to PB (0.1 M, pH 7.4) for 10 minutes and exposed to 1% osmium tetroxide for 20 minutes. They were then rinsed with PB and dehydrated in an increasing gradient of ethanol. Uranyl acetate (1%) was added to the 70% alcohol step in the gradient in order to increase contrast at the electron microscope. The sections were then treated with propylene oxide before being embedded in epoxy resin (Durcupan, ACM; Fluka, Buchs, Switzerland) for 12 hours, mounted on microscope slides, and placed in a 60°C oven for 48 hours.

Control experiments—In a series of control experiments, sections were processed as described above, but without primary antibodies (as a control for the specificity of secondary antibodies). The resulting sections were completely devoid of immunostaining following the incubations.

Ultrathin serial sectioning, electron microscopy analysis, and 3D reconstruction

Blocks of tissue from the postcommissural putamen (six blocks per animal) were taken out from the slides and glued on top of resin blocks with cyanoacrylate glue. These blocks were then trimmed and cut serially into 60-nm ultrathin serial sections with an ultramicrotome (Ultra-cut T2; Leica, Germany), and collected on single-slot Pioloform-coated copper grids. In order to only use tissue with adequate antibody penetration, the electron microscopic analyses were restricted to ultrathin sections from the most superficial sections of blocks. The 3D reconstruction of individual terminals and synapses was performed from elements serially cut through long ribbons (20–30 sections/grid) of ultrathin sections with uniform thickness and good immunostaining. Sections were stained with lead citrate for 5 minutes and examined with Zeiss (Thornwood, NY) EM-10C and JEOL (Peabody, MA) electron microscopes. The serial ultrathin sections of immunoreactive terminals and their corresponding postsynaptic targets (30 profiles/group) were then digitized. Electron micrographs were taken at 16,000× magnification with a CCD camera (DualView 300W; DigitalMicrograph software, version 3.10.1; Gatan, Pleasanton, CA), saved to computer disk, and then aligned and reconstructed in 3D using the *Reconstruct* software application (available at: synapses.clm.utexas.edu).

In order to avoid bias in the selection of elements being reconstructed, the electron microscopic observer was blinded to the treatment (control versus MPTP-treated) and vGluT antibodies (vGluT1 vs. vGluT2) used in the tissue under analysis. Using this approach, the shape and size of the spines, the size (area) of the postsynaptic densities (PSDs), the volume of the spine apparatus (SA), the volume of the spines, and the volume of vGluT1- and vGluT2-immunoreactive terminals were randomly recorded in control and MPTP-treated animals. Only cases in which the spine and the terminal were completely recovered through serial sections were 3D-reconstructed and compared statistically.

To perform this analysis, serial digitized electron microscopic images were converted to TIFF format, imported into *Reconstruct*, calibrated, and aligned. (Aligning was done while ensuring that they were not distorted.) The section thickness was calibrated by using the method of cylindrical diameters (Fiala and Harris, 2001). Finally, the individual contours for the different analyzed objects (spine, PSD, SA, immunoreactive terminal, mitochondria) were manually traced in each serial electron micrograph by using the *Reconstruct* software. The program calculated the dimensions of each object and generated a 3D representation based on the serial slice information. Measurements were made according to criteria used in previous studies for other neuronal populations (Harris and Stevens, 1988, 1989; Harris and Kater, 1994; Arellano et al., 2007; Bourne and Harris, 2008).

Statistical analysis and photomicrograph production

Statistics were performed by using SigmaStat (version 2.03; Aspire Software International, Ashburn, VA). The data from control and MPTP-treated monkeys were analyzed with a one-way ANOVA to determine differences among animals in each group. Data were expressed as mean ± SEM and compared by t-test or Mann-Whitney test to determine statistical differences between control and MPTP-treated monkeys. Pearson Chi-square analysis was used to compare proportions of perforated synapses between normal and MPTP-treated conditions. Pictures were digitally acquired and imported in TIFF format to Adobe Photoshop (version 7.0; Adobe Systems, San Jose, CA) and adjusted only for brightness and contrast, to optimize the quality of the images for analysis.

RESULTS

The extent of striatal dopamine depletion and nigral cell loss in the MPTP-treated animals used in this study has been previously reported (Raju et al., 2008; Villalba et al., 2009). In brief, the whole extent of the caudate nucleus and putamen was almost completely devoid of tyrosine hydroxylase (TH) innervation. Only the nucleus accumbens showed significant immunoreactivity. At the midbrain level, the ventral tier of the substantia nigra pars compacta (SNc) was severely damaged, whereas a significant number of TH-immunoreactive neurons and processes remained in the ventral tegmental area and dorsal tier SNc (Villalba et al., 2009). One-way ANOVAs analysis did not reveal any significant interindividual differences in the extent of striatal spine loss in the different striatal regions between MPTP-treated monkeys used in these studies (Villalba et al., 2009).

Corticostriatal and thalamostriatal axospinous synapses in normal and parkinsonian monkeys

We compared the ultrastructural features of spines contacted by vGluT1-positive terminals with those contacted by vGluT2-immunoreactive boutons to determine structural differences between axo-spinous corticostriatal and thalamostriatal synapses in normal and MPTP-treated monkeys. A series of 120 spines that were randomly selected from vGluT1- or vGluT2-immunostained postcommissural putamen tissue of three normal and three MPTP-treated monkeys (10 spines per monkey/vGluTs antibody) were 3D-reconstructed (Fig. 1A,A1,A2,B,B1). The spine volume, the area of the PSD, and the volume of the presynaptic immunoreactive terminal (vGluT1-IR or vGluT2-IR) making synaptic contact with the spine in control (n = 3) and MPTP-treated (n = 3) animals were measured and averaged from each monkey.

In both control and MPTP-treated animals, there was no significant difference in these measurements (one-way ANOVA) between the three animals in each group, suggesting that the ultrastructural differences observed between the normal and parkinsonian monkeys were due to the MPTP treatment, and that differences between vGluT1- and vGluT2-

immunostained sections were consistent across animals in the same group (Fig. 1C–E). This quantitative analysis of 3D-reconstructed spines revealed that: 1) the volume and the PSDs of spines contacted by corticostriatal terminals were significantly larger than those of spines contacted by thalamostriatal boutons in control and MPTP-treated monkeys (Fig. 1C,D; *, $P < 0.001$; t-test); 2) the vGluT1-positive terminals were significantly larger than vGluT2-positive boutons in control monkeys, but not in parkinsonian animals (Fig. 1C,D; *, $P = 0.016$; t-test); and 3) the volume of the spines, their afferent terminals, and the corresponding PSD areas of cortical (Fig. 1E) and thalamic (Fig. 1F) glutamatergic synapses were significantly larger in parkinsonian monkeys than in controls (*, $P < 0.001$; t-test).

We also found that the sizes of the PSD areas were correlated with spine volumes in spines contacted by vGluT1-IR terminals in control (R 0.815; $P < 0.0001$; n = 30; n = 3; Fig. 2A) and MPTP-treated animals (R = 0.777; $P < 0.0001$; n = 30; n = 3; Fig. 2B). Similar correlations were found for spines receiving vGluT2-IR terminals in the control (R = 0.699; $P < 0.0001$; n = 30; Fig. 2C) and parkinsonian condition (R = 0.724; $P < 0.0001$; n = 30; Fig. 2D).

Changes in the volume of spine apparatus (SA) in parkinsonian condition

Because the SA plays a key role in calcium buffering and protein synthesis (Burgoyne et al., 1983; Fifkova et al, 1983; Steward and Reeves, 1988; Gardiol et al., 1999; Cooney et al., 2002; Horton and Ehlers, 2004; Bourne and Harris, 2008), an expansion of this specialized compartment of the endoplasmic reticulum may have important functional consequences for excitatory transmission at corticostriatal and thalamostriatal synapses. In order to assess potential changes in the SA in the parkinsonian condition, we reconstructed and measured the total volume of the SA in 46 spines contacted by vGluT1- or vGluT2-IR terminals in three control (n = 10 vGluT1, 10 vGluT2) and three MPTP-treated (n =13 vGluT1, 13 vGluT2) monkeys (Fig. 3A–B2).

A one-way ANOVA revealed no significant interindividual difference in SA volume between animals of the same group used in this analysis. There was no significant difference in the relative volume of the SA over the total spine volume (Vol SA/Vol Spi) between spines contacted by cortical or thalamic boutons (Fig. 3C). However, the ratio of the SA volume over the total spine volume was significantly increased in spines targeted by vGluT1-IR cortical terminals, but not by vGluT2-IR thalamic terminals, in MPTP-treated monkeys compared with controls (*, P 0.032; t-test; Fig. 3C), thereby indicating that the enlargement of the SA in vGluT1-contacted spines is not merely the result of the enlargement of vGluT1-recipient spines in the parkinsonian condition.

Increased incidence of perforated and complex postsynaptic densities in the parkinsonian condition

Beside the morphometric quantitative comparison of the total surface of PSDs, we analyzed from 3D-reconstructed images the morphological characteristics (perforated vs. nonperforated/macular) of PSDs in spines receiving vGluT1- or vGluT2-IR inputs in control (n = 3) and MPTP-treated (n = 3) monkeys (Fig. 4). In both control and MPTP-treated animals, almost 100% of PSDs examined at vGluT1-containing synapses (n = 30 PSDs in control and MPTP-treated animals) were perforated, whereas for vGluT2-positive synapses (n = 30 synapses in control and MPTP-treated animals), 83% displayed this ultrastructural feature in normal monkeys, and 90% did so in MPTP-treated animals (Fig. 4E).

Although most glutamatergic axo-spinous synapses are perforated in both normal and parkinsonian conditions in primates, our 3D analysis revealed a much higher level of complexity and an increased number of perforations of the PSDs at glutamatergic axo-

spinous synapses in MPTP-treated monkeys (Fig. 4). In order to quantify this structural remodeling, we compared the number of perforations in PSDs from spines contacted by vGluT1- (n = 51) or vGluT2-IR (n = 52) terminals in control (n = 3) and MPTP-treated (n = 3) animals (Fig. 4F). The statistical analysis showed that in MPTP-treated animals there was a significant increase in the proportion of PSDs with more than two perforations (complex PSDs) in spines contacted by either vGluT1- (χ^2 4.78; *P* 0.03) and vGluT2-IR (χ^2 = 4.34; *P* = terminals (Fig. 4F).

Multisynaptic innervation of vGluT2-positive terminals in normal and MPTP-treated monkeys

In both control (Fig. 5) and MPTP-treated animals (Fig. 6), the 3D reconstruction of vGluT2-positive terminals identified 5–10% boutons that formed asymmetric synapses with more than one postsynaptic structure; some terminals formed dual synapses with a dendritic shaft and a spine head from the same (Fig. 5A,A1,A2) or a different dendrite (Fig. 5B,B1). In other instances, single vGluT2-positive terminals formed asymmetric synapses with multiple spines (Fig. 6A′,A″). These different forms of multisynaptic innervation of postsynaptic targets were not encountered for any of the 60 serially reconstructed vGluT1-positive corticostriatal terminals in normal or MPTP-treated monkeys (see supplementary video).

Changes in mitochondria versus terminal volumes in corticostriatal terminals of parkinsonian monkeys

Mitochondria in the axon terminal are critical for the mobilization of the reserve pool of synaptic vesicles and for the regulation of synaptic strength (Verstreken et al., 2005). Changes in the size and number of mitochondria have been characterized as indices of activity in the axon terminal and synaptic strength by using various in vivo (crayfish motoneurons) and in vitro (Drosophila neuromuscular junction and rat neuronal cortical cultures) neuronal preparations (Lnenicka et al., 1998; Rintoul et al., 2003; Verstreken et al., 2005; Tong, 2007). To determine whether such changes also occur in striatal glutamatergic terminals in the parkinsonian condition, we 3D-reconstructed and compared statistically the volume of the mitochondria in 12 vGluT1- and 12 vGluT2-IR terminals between control (n = 3) and MPTP-treated (n = 3) monkeys (Fig. 7). The qualitative analysis of the =3D-reconstructed images showed that most of the vGluT1-IR terminals from MPTP-treated animals contained a larger number of smaller mitochondria (Fig. 7B) than those from control monkeys (Fig. 7A), whereas this difference was not observed for vGluT2-IR terminals.

Our quantitative analysis confirmed those results, showing an increased number of mitochondria with a smaller volume in MPTP-treated monkeys compared with controls (*, *P* = 0.024; Mann-Whitney test; Fig. 7C,E). In contrast, vGluT2-IR terminals showed no statistically significant change in the number of mitochondria per terminal between normal and parkinsonian condition (Fig. 7D,F).

DISCUSSION

Our study demonstrates three major ultrastructural features related to the morphology and plasticity of glutamatergic axo-spinous synapses in the primate striatum that may underlie functional differences between the corticostriatal and thalamostriatal systems in normal and parkinsonian monkeys. First, the dendritic spines targeted by vGluT1-containing terminals are significantly larger and harbor a more extensive postsynaptic density than those innervated by vGluT2-positive boutons. Combined with their differential expression in vGluTs (Raju and Smith, 2005; Raju et al., 2006, 2008) and specific physiological properties

(Ding et al., 2008), these data suggest that the cerebral cortex and thalamus are two main sources of neurochemically and functionally distinct glutamatergic afferents to the monkey striatum (Smith et al., 2004, 2009a,b).

Second, a subset of vGluT2-positive terminals displays a pattern of multisynaptic connectivity, thereby suggesting that information from single vGluT2-positive axon terminals can be transmitted through multiple synaptic sites on the same or different striatal neurons, a pattern that has not been observed for corticostriatal boutons in normal or parkinsonian condition.

Third, corticostriatal axo-spinous synapses in the sensorimotor putamen of parkinsonian monkeys undergo complex ultrastructural remodeling consistent with increased synaptic activity (larger spine volume, larger PSDs, increased number of PSD perforations, larger pre-synaptic terminal, larger spine apparatus, increased number and decreased volume of terminal mitochondria). Although some of these plastic changes also characterized vGluT2-positive axo-spinous synapses (larger spine volume, larger PSDs, increased number of PSD perforations), others were specific to cortical afferents. Together with various electrophysiological studies suggesting over-activity of the corticostriatal system in rodent and nonhuman primate models of parkinsonism (Galarraga et al., 1987; Marti et al., 1999; Gubellini et al., 2002; Liang et al., 2008), these data illustrate the complex level of synaptic plasticity that governs striatal glutamatergic transmission under normal and parkinsonian conditions.

Anatomical and functional characteristics of corticostriatal versus thalamostriatal glutamatergic systems

Although the functional significance of the dual corticostriatal and thalamostriatal glutamatergic systems remains poorly understood, major advances have been made in our understanding of the anatomical organization and synaptic relationships of these extrinsic inputs with striatofugal neurons (Smith et al., 2004, 2009b). Through the use of anterograde tracing methods and vGluT immunocytochemistry, it is now well established that dendritic spines are the preferential targets of both cortical and thalamic inputs to the striatum (Lacey et al., 2005; Raju et al., 2006, 2008; Smith et al., 2009a,b). However, the synaptology of the thalamostriatal system is complex and differs depending on its nuclear origin so that afferents from the caudal intralaminar nuclei, the center median and parafascicular nuclei (CM/Pf), terminate mainly on dendritic shafts of striatofugal neurons, whereas inputs from other sensorimotor and associative/limbic thalamic nuclei target almost exclusively dendritic spines (Smith et al., 2004, 2009a,b; Raju et al., 2006; Lacey et al., 2007).

The findings of the present study add a further level of complexity to this organization by demonstrating that some vGluT2-positive terminals in the monkey putamen can form dual synapses with both dendritic shaft and dendritic spine, a pattern that has not been described for corticostriatal boutons in both normal and pathological conditions (Kemp and Powell, 1970; Raju et al., 2008). Although neurons in the subthalamic nucleus, hypothalamus, and brainstem regions, known to express vGluT2 (Fremeau et al., 2001, 2004), may be the sources of some of these vGluT2-containing terminals, the massive thalamostriatal system most likely provides the vast majority of striatal vGluT2-positive boutons (Smith et al., 2004, 2009b).

Rodent studies also support a heterogeneous origin of cortical terminals so that excitatory inputs from intratelen-cephalic (IT) cortical neurons terminate in the ipsilateral and contralateral striatum, whereas another contingent of cortical boutons originates from axon collaterals of ipsilateral pyramidal tract (PT) neurons that send their main axons to the brainstem and spinal cord (Lei et al., 2004). However, the translation of this categorization

of corticostriatal terminals to primates must be further explored, and the lack of specific anatomical markers for IT and PT terminals limited our capabilities in differentiating these two types of cortical terminals in the present study.

Despite its more modest extent, the axo-spinous thalamostriatal system displays anatomical features closely related to those of corticostriatal afferents (Raju et al., 2008; Smith et al., 2009a,b). In addition to their synaptic interactions with dendritic spines, both inputs display close association with dopaminergic afferents (Moss and Bolam, 2008). However, recent data indicate that these two systems differ in their neurochemical and electrophysiological properties. The thalamostriatal terminals express vGluT2 and display a higher release probability for glutamate than vGluT1-containing corticostriatal terminals, suggesting a differential degree of short-term plasticity between these two glutamatergic systems (Ding et al., 2008). In addition, thalamostriatal and corticostriatal synapses diverge in their relative expression of NMDA and AMPA glutamate receptors, with a significantly larger NMDA/AMPA ratio at corticostriatal than thalamostriatal synapses in mouse brain slices (Ding et al., 2008; but see Smeal et al., 2008).

Although the correlation between spine morphology and synaptic properties remains poorly understood in the striatum, it is clear from data gathered in the hippocampus (Harris and Kater, 1994; Harris, 1999, Sorra and Harris, 2000; Bourne and Harris, 2008), that larger volumes of spines and postsynaptic densities, as shown for cortical terminals over thalamic boutons in our study, are suggestive of higher strength of the corticostriatal synapses over axo-spinous thalamostriatal synapses in the primate putamen. Future studies that directly assess the number of glutamate receptors at cortical versus thalamic synapses, and determine changes in the electrophysiological properties of thalamostriatal and corticostriatal pathways under normal and parkinsonian conditions, are warranted to test this hypothesis. It is also important to keep in mind that a significant proportion of the thalamostriatal system that originates from the caudal intralaminar nuclei is preferentially directed at dendritic shafts, and that the ultra-structural, neurochemical, and plastic properties of this system in normal and pathological conditions remain to be examined (Smith et al., 2004, 2009a,b). Finally, another essential issue that remains to be determined is whether the ultrastructural remodeling of glutamatergic synapses described in this study similarly affects direct versus indirect striatofugal neurons.

Changes in PSDs, spine apparatus, and terminal mitochondria in parkinsonian monkeys

In line with early rodent and human data suggesting morphological changes of asymmetric synapses in the parkinsonian striatum (Ingham et al., 1993, 1998; Anglade et al., 1996; Ingham et al., 1998; Meshul et al., 1999, 2000), our ultrastructural data demonstrate that the size of the PSD area at axo-spinous cortico- and thalamostriatal synapses is increased in the nonhuman primate model of PD, thereby suggesting that both thalamic and cortical inputs undergo plastic changes consistent with increased synaptic strength in parkinsonism (Harris and Kater, 1994; Harris, 1999, Sorra and Harris, 2000; Bourne and Harris, 2008). However, although evidence for increased synaptic activity at cortical synapses has been proposed by some authors in rodent models of parkinsonism (Galarraga et al., 1987; Marti et al., 1999; Gubellini et al., 2002; Liang et al., 2008), the physiological properties of thalamostriatal axo-spinous synapses in parkinsonian condition remain to be established.

In addition to a size increase, PSDs at cortical and thalamic synapses are much more complex and display a larger number of perforations in the putamen of parkinsonian monkeys. In the hippocampus, the development of segmented or completely partitioned PSDs has been considered as structural modifications associated with increased synaptic efficacy and learning (Nieto-Sampedro et al., 1982; Lisman and Harris, 1993). The exact mechanisms underlying these functional changes are not known, but it has been

hypothesized that the compartmentalization of multiple transmission zones impedes the saturation of postsynaptic receptors and allows multiple transmitter quanta to be effective at the same postsynaptic spine, thereby enhancing the strength of individual synapses (Lisman and Harris, 1993). Thus, the extensive remodeling of PSDs at glutamatergic axo-spinous synapses in the striatum of parkinsonian monkeys provides another mechanism whereby cortical and thalamic glutamatergic afferents may increase their synaptic strength in parkinsonism.

Another striking change observed in spines that receive vGluT1-containing cortical inputs in the striatum of MPTP-treated monkeys is the massive growth of the spine apparatus at corticostriatal synapses. These changes are consistent with increased protein synthesis and increased buffering of intraspinous calcium at glutamatergic synapses in other brain regions (Fifkova et al., 1983; Steward and Reeves, 1988; Gardiol et al., 1999; Toni et al., 2001; Cooney et al., 2002; Horton and Ehlers, 2004; Bourne and Harris, 2008), thereby providing further evidence for increased corticostriatal glutamatergic transmission in the parkinsonian condition (Galarraga et al., 1987; Calabresi et al., 1996; Marti et al., 1999; Gubellini et al., 2002).

Finally, mitochondria in axon terminals are the sources of energy production that is particularly important for the mobilization of the reserve pool of synaptic vesicles and the control of synaptic plasticity and strength (Lnenicka et al, 1998; Rintoul et al., 2003; Verstreken et al., 2005; Tong, 2007). The shortening in the volume and the increased number of mitochondria in cortical boutons of parkinsonian monkeys suggest a higher mitochondrial traffic along corticostriatal axons (Verstreken et al., 2005; Safiulina et al., 2006), probably due to a higher activity and energetic demand at corticostriatal synapses in the parkinsonian condition.

CONCLUSIONS

Our findings highlight the dynamic nature of striatal spine morphology, and provide insights into the complex and multifaceted regulation of compensatory structural changes in corticostriatal and thalamostriatal glutamatergic systems in parkinsonism. Information regarding the molecular and neurochemical mechanisms that regulate striatal spinogenesis and functional studies of the corticostriatal and thalamostriatal systems in normal and parkinsonian conditions are needed to better understand the potential roles that striatal spine remodeling plays in the pathophysiology of PD.

Supplementary Material

Refer to Web version on PubMed Central for supplementary material.

Acknowledgments

The authors thank Jean-Francois Pare for his expert technical assistance with serial electron microscopy sections. Thanks are also due to Drs. Thomas Wichmann and Adriana Galvan for critical reading of the manuscript. The authors also thank the Yerkes Center Animal Resources Division for help with the care of MPTP-treated monkeys.

Grant sponsor: the National Institutes of Health; Grant number: R01 NS 037948 (to Y.S.); Grant sponsor: the National Center for Research Resources-Yerkes Primate Center; Grant number: RR00165.

LITERATURE CITED

Anglade P, Mouatt-Prigent A, Agid Y, Hirsch E. Synaptic plasticity in the caudate nucleus of patients with Parkinson's disease. Neurodegeneration 1996;5:121–128. [PubMed: 8819132]

Arellano JB, Yousef YA, Melo TB, Mohamad SB, Cogdell RJ, Naqvi KR. Formation and geminate quenching of singlet oxygen in purple bacterial reaction center. J Photo-chem Photobiol B 2007;87:105–112.

Bacci JJ, Kachidian P, Kerkerian-Le Goff L, Salin P. Intralaminar thalamic nuclei lesions: widespread impact on dopamine denervation mediated cellular defects in the rat basal ganglia. J Neuropathol Exp Neurol 2004;63:20–31. [PubMed: 14748558]

Ballion B, Mallet N, Bezard E, Lanciego JL, Gonon F. Intratelencephalic neurons equally excite striatonigral and striatopallidal neurons and their discharge activity is selectively reduced in experimental parkinsonism. Eur J Neurosci 2008;27:2313–2321. [PubMed: 18445222]

Bamford NS, Robinson S, Palmiter RD, Joyce JA, Moore C, Meshul CK. Dopamine modulates release from corticostriatal terminals. J Neurosci 2004;24:9541–9552. [PubMed: 15509741]

Bertoni-Freddari C, Fattoretti P, Casoli T, Spagna C, Meier-Ruge W, Ulrich J. Compensatory enlargement of synaptic size in aging and senile dementia. Boll Soc Ital Biol Sper 1993;69:57–63. [PubMed: 8329192]

Bogenpohl, J.; Pare, JP.; Smith, Y. Subcellular localization of adenosine A2A receptors in the striatum and globus pallidus of monkey and rat. IX Triennial Meeting of the International Basal Ganglia Society; 2007.

Bourne JN, Harris KM. Balancing structure and function at hippocampal dendritic spines. Annu Rev Neurosci 2008;31:47–67. [PubMed: 18284372]

Burgoyne RD, Barron J, Geisow MJ. Cytochemical localisation of calcium binding sites in adrenal chromaffin cells and their relation to secretion. Cell Tissue Res 1983;229:207–217. [PubMed: 6831543]

Calabresi P, Pisani A, Mercuri NB, Bernardi G. The corticostriatal projection: from synaptic plasticity to dysfunctions of the basal ganglia. Trends Neurosci 1996;19:19–24. [PubMed: 8787136]

Calabresi P, Picconi B, Tozzi A, Di Filippo M. Dopaminemediated regulation of corticostriatal synaptic plasticity. Trends Neurosci 2007;30:211–219. [PubMed: 17367873]

Cooney JR, Hurlburt JL, Selig DK, Harris KM, Fiala JC. Endosomal compartments serve multiple hippocampal dendritic spines from a widespread rather than a local store of recycling membrane. J Neurosci 2002;22:2215–2224. [PubMed: 11896161]

Day M, Wang Z, Ding J, An X, Ingham CA, Shering AF, Wokosin D, Ilijic E, Sun Z, Sampson AR, Mugnaini E, Deutch AY, Sesack SR, Arbuthnott GW, Surmeier DJ. Selective elimination of glutamatergic synapses on striatopallidal neurons in Parkinson disease models. Nat Neurosci 2006;9:251–259. [PubMed: 16415865]

Deutch AY, Colbran RJ, Winder DJ. Striatal plasticity and medium spiny neuron dendritic remodeling in parkinsonism. Parkinsonism Relat Disord 2007;13(suppl 3):S251–258. [PubMed: 18267246]

Ding J, Peterson JD, Surmeier DJ. Corticostriatal and thalamostriatal synapses have distinctive properties. J Neurosci 2008;28:6483–6492. [PubMed: 18562619]

Fiala JC, Harris KM. Cylindrical diameters method for calibrating section thickness in serial electron microscopy. J Microsc 2001;202:468–472. [PubMed: 11422668]

Fifkova E, Markham JA, Delay RJ. Calcium in the spine apparatus of dendritic spines in the dentate molecular layer. Brain Res 1983;266:163–168. [PubMed: 6189559]

Fremeau RT Jr, Troyer MD, Pahner I, Nygaard GO, Tran CH, Reimer RJ, Bellocchio EE, Fortin D, Storm-Mathisen J, Edwards RH. The expression of vesicular glutamate transporters defines two classes of excitatory synapse. Neuron 2001;31:247–260. [PubMed: 11502256]

Fremeau RT Jr, Voglmaier S, Seal RP, Edwards RH. VGLUTs define subsets of excitatory neurons and suggest novel roles for glutamate. Trends Neurosci 2004;27:98–103. [PubMed: 15102489]

Galarraga E, Bargas J, Martinez-Fong D, Aceves J. Spontaneous synaptic potentials in dopamine-denervated neostriatal neurons. Neurosci Lett 1987;81:351–355. [PubMed: 3124024]

Galvan A, Hu X, Smith Y, Wichmann T. Localization and function of GABA transporters in the globus pallidus of parkinsonian monkeys. Exp Neurol 2010;223:505–515. [PubMed: 20138865]

Garcia BG, Neely MD, Deutch AY. Cortical regulation of striatal medium spiny neuron dendritic remodeling in parkinsonism: modulation of glutamate release reverses dopamine depletion-induced dendritic spine loss. Cereb Cortex 2010;20:2423–2432. [PubMed: 20118184]

Gardiol A, Racca C, Triller A. Dendritic and postsynaptic protein synthetic machinery. J Neurosci 1999;19:168–179. [PubMed: 9870948]

Greenough WT, West RW, DeVoogd TJ. Subsynaptic plate perforations: changes with age and experience in the rat. Science 1978;202:1096–1098. [PubMed: 715459]

Gubellini P, Picconi B, Bari M, Battista N, Calabresi P, Centonze D, Bernardi G, Finazzi-Agro A, Maccarrone M. Experimental parkinsonism alters endocannabinoid degradation: implications for striatal glutamatergic transmission. J Neurosci 2002;22:6900–6907. [PubMed: 12177188]

Harris KM. Structure, development, and plasticity of dendritic spines. Curr Opin Neurobiol 1999;9:343–348. [PubMed: 10395574]

Harris KM, Kater SB. Dendritic spines: cellular specializations imparting both stability and flexibility to synaptic function. Annu Rev Neurosci 1994;17:341–371. [PubMed: 8210179]

Harris KM, Stevens JK. Dendritic spines of rat cerebellar Purkinje cells: serial electron microscopy with reference to their biophysical characteristics. J Neurosci 1988;8:4455–4469. [PubMed: 3199186]

Harris KM, Stevens JK. Dendritic spines of CA 1 pyramidal cells in the rat hippocampus: serial electron microscopy with reference to their biophysical characteristics. J Neurosci 1989;9:2982–2997. [PubMed: 2769375]

Herzog E, Bellenchi GC, Gras C, Bernard V, Ravassard P, Bedet C, Gasnier B, Giros B, El Mestikawy S. The existence of a second vesicular glutamate transporter specifies subpopulations of glutamatergic neurons. J Neurosci 2001;21(RC181):1–6.

Horton AC, Ehlers MD. Secretory trafficking in neuronal dendrites. Nat Cell Biol 2004;6:585–591. [PubMed: 15232591]

Hur EE, Zaborszky L. Vglut2 afferents to the medial pre-frontal and primary somatosensory cortices: a combined retrograde tracing in situ hybridization. J Comp Neurol 2005;483:351–373. [PubMed: 15682395]

Ingham CA, Hood SH, Arbuthnott GW. Spine density on neostriatal neurones changes with 6-hydroxydopamine lesions and with age. Brain Res 1989;503:334–338. [PubMed: 2514009]

Ingham CA, Hood SH, van Maldegem B, Weenink A, Arbuthnott GW. Morphological changes in the rat neostriatum after unilateral 6-hydroxydopamine injections into the nigrostriatal pathway. Exp Brain Res 1993;93:17–27. [PubMed: 7682182]

Ingham CA, Hood SH, Taggart P, Arbuthnott GW. Plasticity of synapses in the rat neostriatum after unilateral lesion of the nigrostriatal dopaminergic pathway. J Neurosci 1998;18:4732–4743. [PubMed: 9614247]

Kashani A, Betancur C, Giros B, Hirsch E, El Mestikawy S. Altered expression of vesicular glutamate transporters VGLUT1 and VGLUT2 in Parkinson disease. Neurobiol Aging 2007;28:568–578. [PubMed: 16563567]

Kemp JM, Powell TP. The cortico-striate projection in the monkey. Brain 1970;93:525–546. [PubMed: 4990231]

Kliem MA, Pare JF, Khan ZU, Wichmann T, Smith Y. Comparative ultrastructural analysis of D1 and D5 dopamine receptor distribution in the substantia nigra and globus pallidus of monkeys. Adv Behav Biol 2009;58:239–253. [PubMed: 19750130]

Lacey CJ, Boyes J, Gerlach O, Chen L, Magill PJ, Bolam JP. GABA(B) receptors at glutamatergic synapses in the rat striatum. Neuroscience 2005;136:1083–1095. [PubMed: 16226840]

Lacey CJ, Bolam JP, Magill PJ. Novel and distinct operational principles of intralaminar thalamic neurons and their striatal projections. J Neurosci 2007;27:4374–4384. [PubMed: 17442822]

Lei W, Jiao Y, Del Mar N, Reiner A. Evidence for differential cortical input to direct pathway versus indirect pathway striatal projection neurons in rats. J Neurosci 2008;24:8289–8299. [PubMed: 15385612]

Liang L, DeLong MR, Papa SM. Inversion of dopamine responses in striatal medium spiny neurons and involuntary movements. J Neurosci 2008;28:7537–7547. [PubMed: 18650331]

Lisman JE, Harris KM. Quantal analysis and synaptic anatomy–integrating two views of hippocampal plasticity. Trends Neurosci 1993;16:141–147. [PubMed: 7682347]

Lnenicka GA, Arcaro KF, Calabro JM. Activity-dependent development of calcium regulation in growing motor axons. J Neurosci 1998;18:4966–4972. [PubMed: 9634562]

Mallet N, Ballion B, Le Moine C, Gonon F. Cortical inputs and GABA interneurons imbalance projection neurons in the striatum of parkinsonian rats. J Neurosci 2006;26:3875–3884. [PubMed: 16597742]

Marti M, Sbrenna S, Fuxe K, Bianchi C, Beani L, Morari M. In vitro evidence for increased facilitation of striatal acetylcholine release via pre- and postsynaptic NMDA receptors in hemiparkinsonian rats. J Neurochem 1999;72:875–878. [PubMed: 9930765]

Meshul CK, Emre N, Nakamura CM, Allen C, Donohue MK, Buckman JF. Time-dependent changes in striatal glutamate synapses following a 6-hydroxydopamine lesion. Neuroscience 1999;88:1–16. [PubMed: 10051185]

Meshul CK, Cogen JP, Cheng HW, Moore C, Krentz L, McNeill TH. Alterations in rat striatal glutamate synapses following a lesion of the cortico- and/or nigrostriatal pathway. Exp Neurol 2000;165:191–206. [PubMed: 10964498]

Moss J, Bolam JP. A dopaminergic axon lattice in the striatum and its relationship with cortical and thalamic terminals. J Neurosci 2008;28:11221–11230. [PubMed: 18971464]

Neely MD, Schmidt DE, Deutch AY. Cortical regulation of dopamine depletion-induced dendritic spine loss in striatal medium spiny neurons. Neuroscience 2007;149:457–464. [PubMed: 17888581]

Nieto-Sampedro M, Hoff SF, Cotman CW. Perforated postsynaptic densities: probable intermediates in synapse turnover. Proc Natl Acad Sci U S A 1982;79:5718–5722. [PubMed: 6957887]

Raju, DV.; Smith, Y. Differential localization of vesicular glutamate transporters 1 and 2 in the rat striatum. In: Bolam, JP.; Ingham, CA.; Magill, P., editors. Advances in behavioral biology 56. The basal ganglia VIII. Springer; Singapore: 2005. p. 601-610.

Raju DV, Shah DJ, Wright TM, Hall RA, Smith Y. Differential synaptology of vGluT2-containing thalamostriatal afferents between the patch and matrix compartments in rats. J Comp Neurol 2006;499:231–243. [PubMed: 16977615]

Raju DV, Ahern TH, Shah DJ, Wright TM, Standaert DG, Hall RA, Smith Y. Differential synaptic plasticity of the corticostriatal and thalamostriatal systems in an MPTP-treated monkey model of parkinsonism. Eur J Neurosci 2008;27:1647–1658. [PubMed: 18380666]

Rintoul GL, Filiano AJ, Brocard JB, Kress GJ, Reynolds IJ. Glutamate decreases mitochondrial size and movement in primary forebrain neurons. J Neurosci 2003;23:7881–7888. [PubMed: 12944518]

Safiulina D, Veksler V, Zharkovsky A, Kaasik A. Loss of mitochondrial membrane potential is associated with increase in mitochondrial volume: physiological role in neurones. J Cell Physiol 2006;206:347–353. [PubMed: 16110491]

Scholz B, Svensson M, Alm H, Skold K, Falth M, Kultima K, Guigoni C, Doudnikoff E, Li Q, Crossman AR, Bezard E, Andren PE. Striatal proteomic analysis that first L-dopa dose equates to chronic exposure. Plos One 2008;3:e1589. [PubMed: 18270577]

Schuster S, Doudnikoff E, Rylander D, Berthet A, Aubert I, Ittrich C, Bloch B, Cenci MA, Surmeier J, Hengerer B, Bezard E. Antagonizing L-type Ca^{2+} channel reduces development of abnormal involuntary movement in the rat model of L-3,4-dihidroxyphenylalanine-induced dyskinesia. Biol Psych 2009;65:518–526.

Smeal RM, Keefe KA, Wilcox KS. Differences in excitatory transmission between thalamic and cortical afferents to single spiny efferent neurons of rat dorsal striatum. Eur J Neurosci 2008;28:2014–2052.

Smith AD, Bolam JP. The neural network of the basal ganglia as revealed by the study of synaptic connections of identified neurons. Trends Neurosci 1990;3:259–265. [PubMed: 1695400]

Smith Y, Villalba R. Striatal and extrastriatal dopamine in the basal ganglia: an overview of its anatomical organization in normal and parkinsonian brains. Mov Disord 2008;23(Suppl 3):S534–547. [PubMed: 18781680]

Smith Y, Raju DV, Pare JF, Sidibe M. The thalamostriatal system: a highly specific network of the basal ganglia circuitry. Trends Neurosci 2004;27:520–527. [PubMed: 15331233]

Smith Y, Villalba RM, Raju DV. Striatal spine plasticity in Parkinson's disease: pathological or not? Parkinsonism Relat Disord 2009a;15(Suppl 3):S156–161. [PubMed: 20082980]

Smith Y, Raju D, Nanda B, Pare JF, Galvan A, Wichmann T. The thalamostriatal systems: anatomical and functional organization in normal and parkinsonian states. Brain Res Bull 2009b;78:60–68. [PubMed: 18805468]

Soares J, Kliem MA, Betarbet R, Greenamyre JT, Yamamoto B, Wichmann T. Role of external pallidal segment in primate parkinsonism: comparison of the effects of 1-methyl-4-phenyl-1,2,3,6-tetrahydropyridine-induced parkinsonism and lesions of the external pallidal segment. J Neurosci 2004;24:6417–6426. [PubMed: 15269251]

Soderstrom K, O'Malley JA, Levine ND, Sortwell CE, Collier TJ, Steece-Collier K. Impact of dendritic spine preservation in medium spiny neurons on dopamine graft efficacy and the expression of dyskinesias in parkinsonian rats. Eur J Neurosci 2010;31:478–490. [PubMed: 20105237]

Sorra KE, Harris KM. Overview on the structure, composition, function, development, and plasticity of hippocampal dendritic spines. Hippocampus 2000;10:501–511. [PubMed: 11075821]

Stephens B, Mueller AJ, Shering AF, Hood SH, Taggart P, Arbuthnott GW, Bell JE, Kilford L, Kingsbury AE, Daniel SE, Ingham CA. Evidence of a breakdown of corticostriatal connections in Parkinson's disease. Neuroscience 2005;132:741–754. [PubMed: 15837135]

Steward O, Reeves TM. Protein-synthetic machinery beneath postsynaptic sites on CNS neurons: association between polyribosomes and other organelles at the synaptic site. J Neurosci 1988;8:176–184. [PubMed: 3339407]

Surmeier DJ, Ding J, Day M, Wang Z, Shen W. D1 and D2 dopamine-receptor modulation of striatal glutamatergic signaling in striatal medium spiny neurons. Trends Neurosci 2007;30:228–235. [PubMed: 17408758]

Tian X, Kai L, Hockberger PE, Wokosin DL, Surmeier DJ. MEF-2 regulates activity-dependent spine loss in striatopallidal medium spiny neurons. Mol Cell Neurosci 2010;44:94–108. [PubMed: 20197093]

Tong JJ. Mitochondrial delivery is essential for synaptic potentiation. Biol Bull 2007;212:169–175. [PubMed: 17438209]

Toni N, Buchs PA, Nikonenko I, Povilaitite P, Parisi L, Muller D. Remodeling of synaptic membranes after induction of long-term potentiation. J Neurosci 2001;21:6245–6251. [PubMed: 11487647]

Verstreken P, Ly CV, Venken KJ, Koh TW, Zhou Y, Bellen HJ. Synaptic mitochondria are critical for mobilization of reserve pool vesicles at *Drosophila* neuromuscular junctions. Neuron 2005;47:365–378. [PubMed: 16055061]

Villalba RM, Raju DV, Hall RA, Smith Y. GABA(B) receptors in the centromedian/parafascicular thalamic nuclear complex: an ultrastructural analysis of GABA(B)R1 and GABA(B)R2 in the monkey thalamus. J Comp Neurol 2006;496:269–287. [PubMed: 16538684]

Villalba RM, Lee H, Smith Y. Dopaminergic denervation and spine loss in the striatum of MPTP-treated monkeys. Exp Neurol 2009;215:220–227. [PubMed: 18977221]

Wichmann T, Delong MR. Anatomy and physiology of the basal ganglia: relevance to Parkinson's disease and related disorders. Handb Clin Neurol 2007;83:1–18. [PubMed: 18808908]

Zaja-Milatovic S, Milatovic D, Schantz AM, Zhang J, Montine KS, Samii A, Deutch AY, Montine TJ. Dendritic degeneration in neostriatal medium spiny neurons in Parkinson disease. Neurology 2005;64:545–547. [PubMed: 15699393]

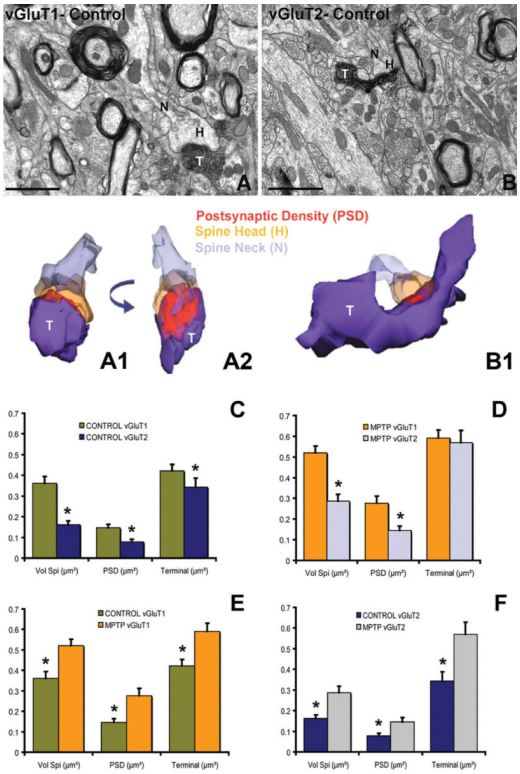

Figure 1.

Ultrastructural features of corticostriatal and thalamostriatal axo-spinous synapses in control and MPTP-treated monkeys. **A,B**: Electron micrographs of vGluT1- (A) and vGluT2- (B) immunoreactive terminals (T) and their postsynaptic spines in the postcommissural putamen of control monkeys. **A1,A2,B1**: 3D reconstruction of the two immunoreactive terminals (T) and their postsynaptic target spines shown in A and B. Both vGluT1- and vGluT2-immunoreactive terminals form asymmetric synapses with the head of the spines. In A2 the 3D-reconstructed image has been rotated with respect to A1 to show the extent and morphology of the postsynaptic density. Partially transparent images of the head of the spine and the terminal allow the visualization of the corresponding perforated (A2) and macular (B1) postsynaptic densities (PSD). C–F: Histograms comparing the morphometric measurements (spine volume, PSD area, terminal volume) of structural elements at corticostriatal and thalamostriatal glutamatergic synapses using the 3D reconstruction method of serial ultrathin sections collected from 30 axo-spinous synapses in each group from three control and three MPTP-treated animals. The units used for these measurements are indicated in the X axis within parentheses. **C**: In control monkeys (n = 3), the spine volume (Vol. Sp), the PSD areas, and the size of presynaptic terminals at corticostriatal synapses are significantly larger than those at thalamostriatal synapses (*, $P < 0.001$ for Vol. Sp. and PSD; *, $P = 0.016$ for terminal; t-test). **D**: The same is true for MPTP-treated monkeys (n = 3), except for the presynaptic terminals that do not display any significant size differences in this condition. *E,F*: The spine volumes, the PSD areas, and the volume of vGluT1- and vGluT2-containing terminals are significantly larger in MPTP-treated parkinsonian monkeys than in controls (*, $P < 0.001$; t-test). Scale bar = 1 µm in A,B. [Color figure can be viewed in the online issue, which is available at wileyonlinelibrary.com.]

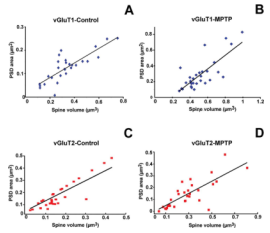

Figure 2.

Scatter diagrams showing the correlation between spine volume (μm^3) and the surface (μm^2) of postsynaptic densities (PSDs) at corticostriatal (vGluT1) and thalamostriatal (vGluT2) excitatory synapses in the postcommissural putamen of normal (n = 3) versus MPTP-treated (n = 3) monkeys. In all cases, the area of the PSDs was positively correlated with the spine volume. **A,B**: Correlation of PSD areas and spine volume in spines that receive vGluT1-containing cortical afferents in control (A; coefficient of correlation, R = 0.815) and MPTP-treated animals (B; R = 0.777). **C,D**: PSD areas plotted as a function of spine volume in striatal spines receiving vGluT2-containing thalamic inputs in normal (C) and parkinsonian monkeys (D). For the correlation between vGluT2-IR terminals and their contacting spines, the value of R was 0.699 for controls and 0.784 for MPTP-treated animals ($P < 0.0001$; the number of spines studied in each group was n = 30 for A–D). [Color figure can be viewed in the online issue, which is available at wileyonlinelibrary.com.]

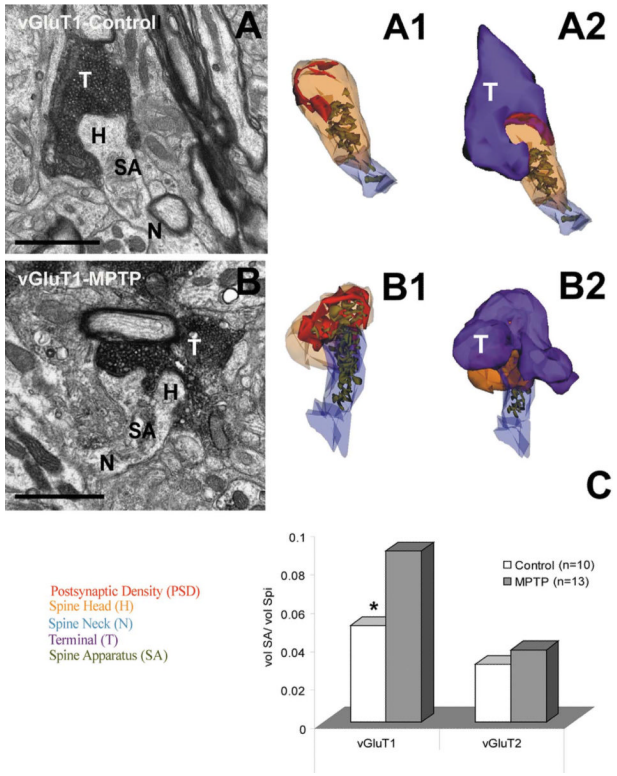

Figure 3.

3D reconstruction and comparative ultrastructural analysis of the spine apparatus (SA) in the striatum of normal (n = 3) and MPTP-treated (n = 3) monkeys. **A,B**: Electron micrographs of vGluT1-immunoreactive axo-spinous synapses in the striatum of control (A) and MPTP-treated (B) monkeys. **A1,A2,B1,B2**: 3D-reconstructed images of the corresponding glutamatergic axo-spinous synapses depicted in A and B from the striatum of control (A,A1,A2) and MPTP-treated (B,B1,B2) monkeys. The neck (N) and head (H) of the spines are partially transparent to better show and compare the complexity and distribution of the SA between control and MPTP conditions. **C**: Histogram comparing the relative volume of the SA over the total spine (Spi) volume in vGluT1- and vGluT2- receiving spines in control and MPTP-treated monkeys. Statistical differences were determined by t-test (*, $P = 0.032$). Scale bar = 1 μm in A,B. [Color figure can be viewed in the online issue, which is available at wileyonlinelibrary.com.]

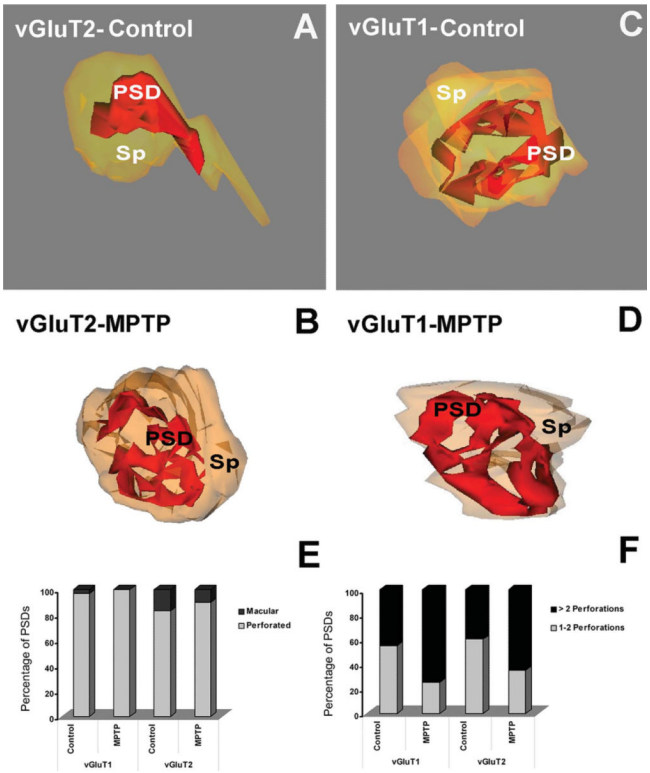

Figure 4.

Morphology of 3D reconstructed individual dendritic spines showing different types and complexity of postsynaptic densities (PSDs). **A,B**: Macular (A) and fenestrated (B) PSDs from spines receiving vGluT2-IR terminals in control (A) and MPTP-treated (B) animals. **C,D**: Perforated (D) and fenestrated (E) PSDs in vGluT1-receiving spines in control (C) and MPTP-treated parkinsonian monkeys (D). **E**: Quantitative analysis of the two types of PSDs (perforated vs. macular) in corticostriatal and thalamostriatal axo-spinous synapses in control (n = 3) and MPTP-treated (n = 3) monkeys. **F**: Comparative analysis of the relative percentages of PSDs with different numbers of perforations in spines contacted by vGluT1- or vGluT2-IR terminals in control (n = 3) and MPTP-treated (n = 3) parkinsonian monkeys. The proportion of complex PSDs (more than two perforations) was significantly increased (Pearson Chi-square analysis, χ^2) in MPTP-treated animals at both corticostriatal ($\chi^2 = 4.78$; $P = 0.03$) and thalamostriatal ($\chi^2 = 4.34$; $P = 0.035$) axo-spinous synapses. Abbreviation: Sp, spine. [Color figure can be viewed in online issue, which is available at wileyonlinelibrary.com.]

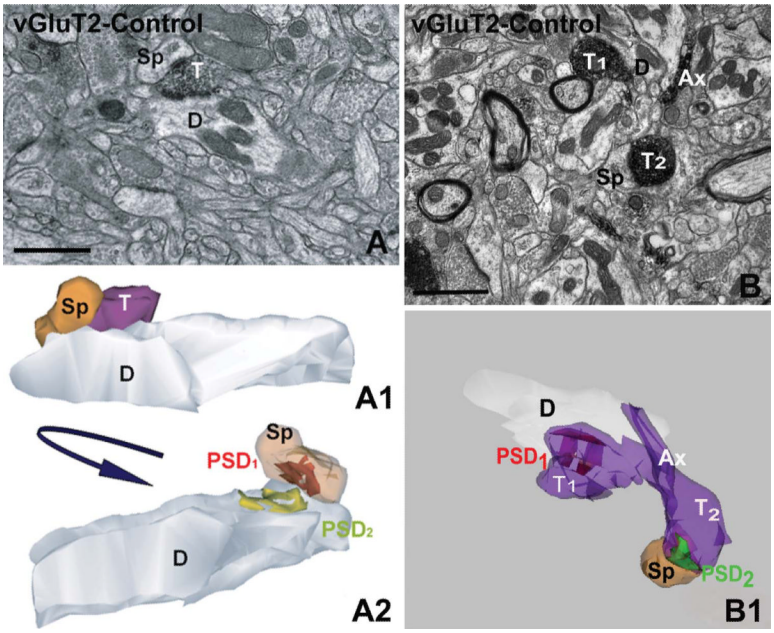

Figure 5.

vGluT2-IR terminals forming dual synapses with dendritic shafts and spines in control animals. **A,B**: Electron micrographs of vGluT2-IR terminals (T,T1,T2) in contact with a dendritic shaft (D) and a spine (Sp) from the same (A1,A2) or different (B1) dendrites. **A1,A2,B1**: 3D reconstructed asymmetric synapses shown in A and B, respectively. The T in A1 forms a synapse with a dendritic shaft (D) and with a sessile spine (Sp) from the same dendrite. However, the vGluT2-IR axon (Ax) depicted in B2 gives rise to two axon terminals (T1 and T2) that form asymmetric synaptic contacts (PSD_1 and PSD_2) with a dendritc shaft (D) and a spine (Sp). The image in A2 has been rotated with respect to A1, and the T has been removed from the image to better illustrate the perforated PSD_1 and PSD_2. Scale bar = 1 μm in A,B. [Color figure can be viewed in the online issue, which is available at wileyonlinelibrary.com.]

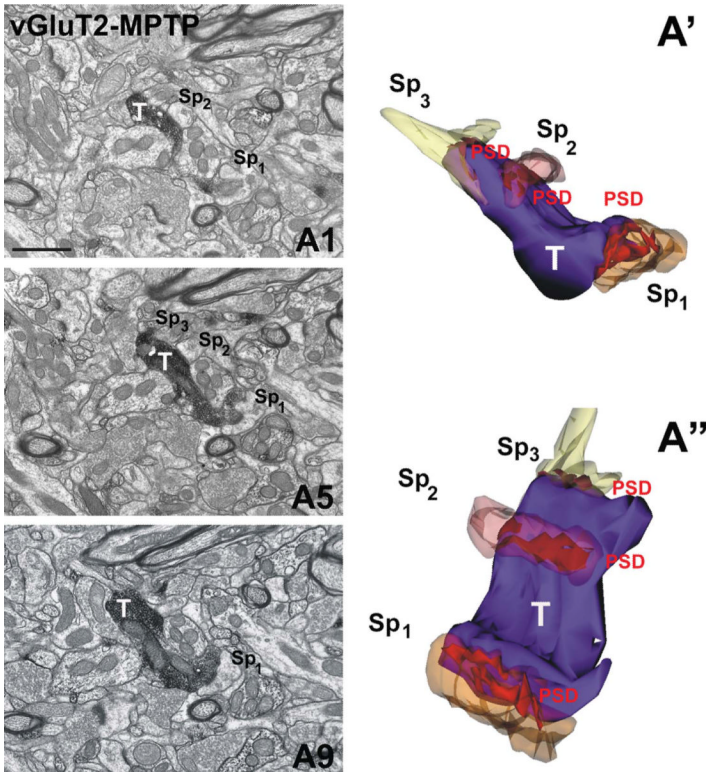

Figure 6.

A vGluT2-IR terminal forming multiple "en passant" type axo-spinous asymmetric synapses in the postcommissural putamen of an MPTP-treated parkinsonian monkey. **A1,A5,A9**: Samples of serial electron micrographs used to generate the 3D reconstructed vGluT2-positive terminal (T) in contact with three different spines (Sp_1, Sp_2, Sp_3)in A′ and A″. Note that the 3D-reconstructed spines (A′ and A″) are partially transparent and the image in A″ is rotated to better illustrate the extent of the postsynaptic densities. Abbreviations: D, dendrite; Sp, spine; PSD, postsynaptic density. Scale bar = 1 μm in A1 (also applies to A5,A9). See supplementary video. [Color figure can be viewed in the online issue, which is available at wileyonlinelibrary.com.]

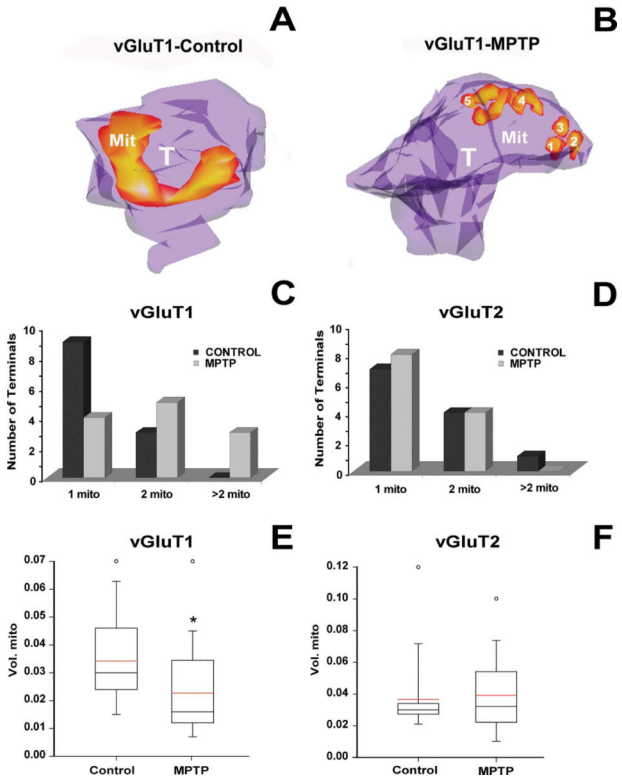

Figure 7.

Number and volume of mitochondria in vGluT1- and vGluT2-immunoreactive terminals in the postcommissural putamen of normal and MPTP-treated parkinsonian monkeys. **A,B**: 3D reconstructed vGluT1-IR terminals (T) in control (A) and MPTP-treated animals (B). These terminals are partially transparent to compare the morphology, number, and distribution of mitochondria (Mit) between control (A) and MPTP-treated monkeys (B). **C,D**: Bar histograms comparing the total number of vGluT1- (C) and vGluT2-IR (D) terminals containing one, two, or three mitochondria in control and MPTP-treated animals. **E,F**: Box diagrams showing the size distribution of mitochondria in vGluT1- (E) and vGluT2-IR (F) terminals. In vGluT1-IR terminals the size of the mitochondria was significantly smaller in MPTP-treated animals than in control (*, $P = 0.024$; Mann-Whitney test; E). No significant differences were found between control and MPTP-treated animals in vGluT2-IR terminals ($P = 0.326$; Mann-Whitney test; F) or between thalamostriatal and corticostriatal terminals in control animals ($P = 0.827$; Mann-Whitney test; E,F). The black line indicates the value of the median, and the red line represents the mean values for each group. The analysis was done in 12 terminals per group from six different animals (3 controls, 3 MPTP-treated). [Color figure can be viewed in the online issue, which is available at wileyonlinelibrary.com.]

TABLE 1

Primary antibodies used

Antigen	Immunogen	Immunizing species	Vendor	Immunooytochemistry concentration
Vesicular glutamate 1 transporter (vGluT1)	COOH terminus rat vGluT1-aa 543–560	Rabbit	MabTechnologies (Atlanta, GA) Catalog No. VGT1-3	0.2 μg/ml
Vesicular glutamate 2 transporter (vGluT2)	COOH terminus human vGluT2-aa 560–578	Rabbit	MabTechnologies (Atlanta, GA) Catalog No. VGT2-6	0.2 μg/ml

TABLE 2

Animal Code and Total Number of Control and MPTP-Treated Monkeys Used for Striatal vGluT1 or vGluT2 Immunostaining

Cortico-striatal (vGluT1)	**Control**	**MPTP**	**animals**
	C1	M1	
	C2	M2	
	C3	***M3***	
Animals used	3	3	**6**
Thalamo-striatal (vGluT2)	**Control**	**MPTP**	
	C2	***M3***	
	C4	M4	
	C5	M5	
Animals used	3	3	**6**
Total animals sacrified	**5**	5	